Surface & Coatings Technology 493 (2024) 131281

Contents lists available at ScienceDirect

Surface & Coatings Technology

journal homepage: www.elsevier.com/locate/surfcoat

Precision depth-controlled isolated silver nanoparticle-doped diamond-like carbon coatings with enhanced ion release, biocompatibility, and mechanical performance

Abdul Wasy Zia [a,*], Ioannis Anestopoulos [b], Leon Bowen [c], Mihalis I. Panayiotidis [b], Martin Birkett [d]

[a] Institute of Mechanical, Process, and Energy Engineering (IMPEE), School of Engineering and Physical Sciences, Heriot-Watt University, Edinburgh, United Kingdom
[b] Department of Cancer Genetics, Therapeutics & Ultrastructural Pathology, The Cyprus Institute of Neurology & Genetics, Nicosia, Cyprus
[c] Department of Physics, G.J. Russell Microscopy Facility, Durham University, Durham, United Kingdom
[d] Faculty of Engineering and Environment, Northumbria University, Newcastle Upon Tyne, United Kingdom

ARTICLE INFO

Keywords:
Diamond-like carbon
Silver
Coating structure
Precision doping
Biomechanical
Sputtering

ABSTRACT

Silver doped diamond-like carbon (Ag/DLC) coatings are in high demand for biomedical applications such as artificial implants, surgical instruments, and medical devices. However, recent reports indicate that the excess Ag concentration required in typically made Ag/DLC coatings significantly reduces their mechanical performance and biocompatibility. Here, we propose a novel single-step approach to precisely dope small quantities of Ag in the form of isolated nanoparticles embedded at defined depths in a DLC matrix. This new Ag/DLC coating architecture is designed to release controlled Ag ion levels to fight infection in the early post-surgery stages, while a confined Ag amount maintains the excellent mechanical and biocompatibility performance of the underlying DLC coating when compared to typically made Ag/DLC coating designs. Coatings of pure DLC, typically made Ag/DLC with Ag doped throughout the carbon matrix and the new Ag/DLC design with precise Ag doping, are made using a modified magnetron sputtering system. The coatings are characterised for structural, mechanical, ion leaching, and biocompatibility profiles against L929 fibroblast cells. Results indicate that the new Ag/DLC coating requires only 2 at.% Ag to release a similar level of Ag ions (~0.6 ppm) to a typical Ag/DLC coating with a much higher Ag content of 17 at.%. The new Ag/DLC coating design also outperforms the typical design with a 63 % increase in hardness, 100 % higher Young's modulus, and 21 % higher biocompatibility. The enhanced biomechanical performance of the proposed new Ag/DLC architecture could have significant potential for coating of future medical devices.

1. Introduction

Diamond-like carbon (DLC) coatings are recognized for their high hardness and Young's modulus, low friction coefficient and wear rates, ultra-smooth surface morphology, and intrinsic biocompatibility [1]. Therefore, these coatings are widely used for biomedical applications, such as artificial implants, surgical instruments, medical textiles and medical devices. DLC coatings lack in self-regulating inflammatory reactions irrespective of their superior mechanical, tribological, and biomedical performance. Hence, metal ions such as silver (Ag), are used to boost their biological functioning. Ag nanoparticles are widely used in the health sector and a breakdown [2] suggests that 52 % of Ag nanoparticles are utilized in health and fitness, 10 % in cleaning, 10 % in food, and the remainder in miscellaneous applications.

Silver doped diamond-like carbon (Ag/DLC) coatings are attractive for medical implants as they provide antimicrobial and antibacterial features, unwanted biological growth inhibition, hemocompatibility, resistance against biofouling and also reduce residual stresses in DLC coatings to ensure their long life. Ag/DLC coatings are typically made with physical vapour deposition (PVD) and plasma-enhanced chemical vapour deposition (PECVD) methods. The DLC is deposited by sputtering or reactive sputtering methods while Ag is doped into a DLC matrix with simultaneous co-sputtering [3]. Although the addition of Ag reduces residual stresses in the DLC matrix and improves its biomedical

* Corresponding author.
E-mail address: a.zia@hw.ac.uk (A.W. Zia).

https://doi.org/10.1016/j.surfcoat.2024.131281
Received 18 June 2024; Received in revised form 19 August 2024; Accepted 20 August 2024
Available online 22 August 2024

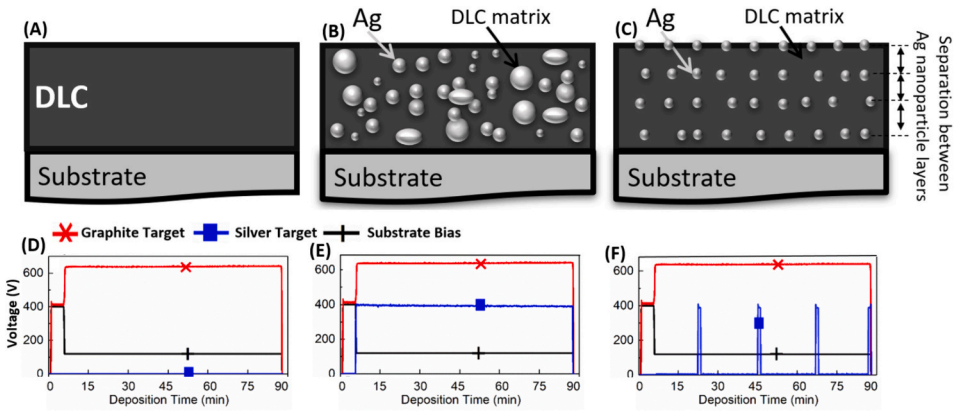

Fig. 1. Schematic of (A) pure DLC (without Ag), (B) typical Ag/DLC design, and (C) proposed new Ag/DLC design. Correspondingly, (D), (E), and (F) present voltage control of graphite and silver targets and substrate bias to deposit pure DLC, typical Ag/DLC and new Ag/DLC coatings. The new Ag/DLC design is attributed with localized doping of a precise amount of Ag at controlled depths in the DLC matrix using power supply and shutter control. This new Ag/DLC coating design maintains biological function without compromising mechanical properties, contrary to typically made Ag/DLC coatings.

performance, it can also result in a significant reduction of mechanical strength. Ag/DLC studies by Wang et al. [4] suggest that adding Ag up to 14 %, reduces the DLC coating hardness from 13.3 to 6.1 GPa (a 54 % decline) and Young's modulus from 165 to 124 GPa (a 25 % decline). Ag/DLC studies performed by Domínguez-Meister et al. [5] suggest that the addition of 17 at.% Ag improves tribological performance by reducing friction coefficient from 0.22 to 0.15 and specific wear rate from 3.0 to 2.6 $\times$ 10^7 mm^3/Nm. However, the coating hardness reduces from 17 to 7 GPa (a 58 % decline) and Young's modulus from 180 to 100 GPa (a 44 % decline). Our preliminary studies [6] report the performance of typical Ag/DLC coatings where Ag is doped as 17, 40, and 65 at.% in a carbon matrix. It was observed that the coating hardness is reduced by 50 % with the addition of 17 at.% Ag and continue to decline with further addition of Ag in a carbon matrix.

Similarly, excess Ag doping not only reduces mechanical function but is also harmful to some biomedical properties. Ag/DLC studies performed by Orrit-Prat et al. [7] suggest doping 2 % Ag into the DLC matrix as a safe proportion to maintain a non-cytotoxic profile for the coating. DLC coatings with higher Ag doping amounts lose biocompatibility and become cytotoxic to human cells and the Ag ion contact-killing mechanism is well demonstrated in the literature [8,9] for red blood cells, bronchial epithelial cells, and keratinocytes etc. [10]. Hence, the amount of Ag doped in the DLC matrix needs to be optimized for the desired specific functioning and working environments such as invasive or non-invasive implants or load-carrying or non-load carrying implants, to maintain a balance between such biological functioning, mechanical strength, and tribological performance. However, current Ag/DLC coating designs that are optimized for biological function usually result in compromised mechanical properties and vice-versa. Whereas load-carrying invasive implants essentially require an optimum combination of both biological and mechanical properties for superior bio-mechanical functioning to reduce the risk of implant-associated infections and extend the lifetime of the device.

Literature studies have mostly investigated Ag/DLC as a function of Ag proportion doped into a DLC matrix and mapped their efficacy against cell viability [11]. However, it is perceived that the amount of Ag ions released from Ag/DLC coatings is a key parameter instead of Ag proportion doped in Ag/DLC coating to perform the required antibiotic, germicidal, and other prophylactic actions. In general, the Ag ion concentration increases with increasing Ag contents doped into the coatings [5] and their corresponding antimicrobial performance also increases. However, it is well known that ion release rate is highly dependent on particle morphologies and surface area, and small-sized Ag nanoparticles have shown higher ion release rates than large nanoparticles, clusters, and agglomerations [12]. The morphology and distribution of Ag also vary with the Ag/DLC coating growth which depends on deposition conditions like bias voltage, chamber pressure, and other relevant operational conditions [13]. It is observed that the Ag nanoparticles are well distributed in soft DLC coatings when compared with hard DLC coatings, which are usually deposited under high substrate bias voltage where the dense and hard carbon microstructure restricts doping of Ostwald ripening and surface segregation [13] grown Ag particles into the DLC matrix. Additionally, the thermal activation and diffusion of Ag are combined factors to segregate Ag at the coating surface [13]. Further, Ag is shown to agglomerate on top of the coating surface during emersion [14] which also hinders it's in vivo functioning. Similarly, a typical co-sputtering process gives less control over the size, morphology, and distribution of Ag in the DLC matrix. Typically Ag/DLC coating designs made with conventional co-sputtering of a graphite target with Ag inclusions have shown a significant variation in Ag particle sizes, soot, clusters, and agglomerations.

Considering poor control over Ag morphologies and distributions in typical Ag/DLC coatings which imperils biomechanical performance, there is a need to re-configure Ag/DLC coating structure where Ag should be doped; (1) in the amount implicitly required for biological functioning, (2) with control over size, morphology, distribution, and depth, giving localized doping of Ag in the DLC matrix, and (3) with minimum compromise on mechanical performance. Recent attempts to dope Ag into DLC have demonstrated control over Ag particle size by regulating plasma kinetics such as bias voltage, assistive energies, and pressures. Ag doped with a gas aggregation cluster source into sputtered DLC has produced 11 nm sized Ag nanoparticles at 100 Pa while bimodal sizes of 31 and 260 nm Ag particles were achieved at 200 Pa [15]. The cluster source beams are reported to dope Ag nanoparticles in small concentrations and size range between 2 and 6 nm in amorphous carbon coatings [16]. In the same way, an increase in assistive energy from 0 to 300 eV has shown a reduction in Ag nanocluster size from ~30 to ~5 nm [17]. Similarly, applying a negative bias voltage to the Ag target and substrate has been shown to regulate Ag flux to control Ag nanoparticle size [13]. The ongoing developments have demonstrated multiple techniques [18] to control Ag nanoparticle size but still lack in localized Ag doping to give control over Ag ion release and enhance bio-mechanical performance of DLC coatings.

Our group is investigating the optimum amount of Ag in DLC coating by formulation, material- and structural design, and manufacturing process to concurrently maintain superior biocompatibility while performing desired antimicrobial actions. In continuation of our research on this theme [6,19], this work proposes a new one-step economical deposition process for controlled synthesis of Ag nanoparticles and their precise embedding in a DLC matrix. We demonstrate the deposition of

Ag/DLC coatings made with 'typical' and 'new' designs for similar Ag ion release rates. In typically deposited Ag/DLC coatings, Ag is three-dimensionally doped into the carbon matrix, with limited control over Ag morphology, growth, and distribution. Therefore, Ag exists in the form of particles, clusters, and agglomerations which compromise the overall biomechanical performance of the Ag/DLC coating. Whereas, in the proposed new Ag/DLC coating design, isolated Ag nanoparticles are doped in two-dimensional planes with controlled interplanar distance. The isolated Ag nanoparticles having larger surface area per unit volume are likely to release more Ag ions when compared to Ag agglomeration and clusters. In addition, doping lower Ag amount in the carbon matrix is also expected to reduce the compromise on mechanical properties. The corresponding structural, mechanical, and biocompatibility studies are performed to understand the significance of this new Ag/DLC design over the typical Ag/DLC design. The new design suggests doping Ag as low as 2 at.% produces a similar biocompatibility profile as delivered by a typically made 17 at.% Ag/DLC coating, with a 63 % and 100 % increase in hardness and Young's modulus, respectively.

The inception of a new Ag/DLC design is based on Ag ion release rates instead of Ag concentrations doped into the DLC matrix. Manninen et al. [20] have demonstrated higher Ag ion release rates from Ag/DLC coatings when compared to pure (amorphous) Ag coatings. Their work shows that the difference in Ag ion release rates from Ag/DLC and pure Ag coatings could be as high as 100 % after leaching periods of 24 h and the higher ion release rate in Ag/DLC coatings is attributed to the formation of galvanic pairs formed between Ag and carbon atoms. Whereas, the slower release of Ag ions from the pure Ag coatings are attributed to interplay between van-der-Waals forces and Gibbs free energy between Ag grains and corresponding grain boundaries [20]. The ion release kinetics become a motivation to re-configure the Ag/DLC coating structural design in this work. Fig. 1 presents the schematic of a pure DLC coating (Fig. 1A), a typically deposited Ag/DLC coating (Fig. 1B), and the structural re-configuration of the proposed new Ag/DLC design (Fig. 1C). Hypothetically, the new Ag/DLC design with (1) a small amount of Ag, (2) doped as spherical nanoparticles of controlled size and distribution, (3) at defined depths in the DLC matrix for time-release action, (4) may have the ability to give similar biological functioning as delivered by typical Ag/DLC coating doped with a larger Ag amount. If successful, (5) the new Ag/DLC design will have the perceived benefit of retaining mechanical performance of the coating which is compromised in the typical Ag/DLC design.

2. Materials and methods

2.1. Deposition of coatings

Pure DLC, typical Ag/DLC, and new Ag/DLC coatings were deposited on standard glass slides (Fisherbrand™) of 76 × 26 × 1 mm by length, width, and thickness. The glass substrates were cleaned with ethanol and dried with pressurized nitrogen. A direct-current magnetron sputtering system (UDP350, Teer Coating Ltd. United Kingdom) was used to deposit DLC and Ag/DLC coatings. The instrument hosts 4 magnetrons, one of them was used for a rectangular graphite target (248 × 133 × 10 mm by length, width, and thickness) and another was used for a circular Ag target (100 × 6.35 mm by diameter and thickness). The deposition process for all coatings remained the same except for doping Ag into the DLC matrix for typical and new Ag/DLC coating designs. Firstly, the glass substrates were loaded into the deposition chamber and it was evacuated to a base pressure of 5 mPa. Prior to deposition, the glass substrates were plasma cleaned for 5 min at a bias voltage of 450 V and current of 0.2 A and Ar flow rate of 0.03 l/min. All coatings were deposited for 90 min at a substrate rotation speed of 2 rpm, Ar gas flow rate of 0.03 l/min, substrate bias of 120 V, chamber pressure of ~0.4 Pa, and graphite target current of 2.0 A and Ag target current of 0.05 A, respectively, to achieve an average thickness of 550 nm. Fig. 1D to F presents the control over target operation to deposit pure DLC, typical Ag/DLC, and new Ag/DLC coatings, respectively. Fig. 1D presents the consistent graphite target voltage over the deposition time to deposit the pure DLC coating design depicted in Fig. 1A. Whereas Fig. 1E presents the consistent target voltages of graphite and Ag targets to co-sputter Ag and graphite to fabricate the typical Ag/DLC design as illustrated in Fig. 1B. Fig. 1F present the consistent graphite target voltage but controlled Ag target voltage to deposit a new Ag/DLC design corresponding to Fig. 1C. The Ag target was turned ON at four specific time instances of 22.5, 45.0, 67.5, and 90.0 min (for 90 s each time) during the 91.5 min long Ag/DLC deposition. Once the Ag plasma plume had stabilised, shutter control was used to expose the specimens to the Ag target for a precise 45 s duration. The voltage peaks in Fig. 1F correspond to the 90 s of Ag target operation ON/OFF as logged by the deposition system in real-time mode.

2.2. Preparation of leached extracts for ion release measurements and biocompatibility profiling

Leached extracts of pure DLC, typical and new Ag/DLC coatings were prepared to measure the release of Ag ion concentrations and biocompatibility profiles against murine fibroblast L929 cells as described below.

2.2.1. Leached extracts prepared to measure Ag ion concentrations

A 50 ml Dulbeccos's Modified Eagle Medium (DMEM) solution including 10 % fetal bovine serum (FBS), 100 μg/ml streptomycin and 100 U/ml penicillin was used to obtain extracts of leached ions of polished (i) copper (Cu), (ii) Titanium (Ti), (iii) pure DLC, (iv) typical Ag/DLC, and (v) new Ag/DLC coating samples of 19 × 25 mm dimensions. The materials under investigation were leached for 72 h and 168 h in a humidified incubator at 37 °C and 5 % CO_2. The blank DMEM was used to prepare four calibration standard solutions having Cu, Ti, and Ag in concentrations of 0.625, 2.5, 5.0, and 10.0 ppm. A commercially available Claritas PPT® Multi-Element Standard for instrument calibration by SPEX CertiPrep, USA was used for this purpose.

2.2.2. Leached extracts prepared for biocompatibility profiling

A DMEM solution was prepared with the addition of 10 % FBS, 100 U/ml penicillin and 100 μg/ml streptomycin. Four types of extracts were prepared in compliance with biocompatibility experiments: (1) 72 h leaching in undiluted DMEM, (2) 168 h leaching in undiluted DMEM, (3) 72 h leaching and 50 % diluted with fresh DMEM, (4) 168 h leaching and 50 % undiluted with fresh DMEM. Polished Cu and medical grade Ti specimens of 19 × 25 mm by length and width were used as positive and negative controls, respectively. The extracts of Cu, Ti metals and pure DLC, typical Ag/DLC and new Ag/DLC coatings were prepared by immersing their coupons in a 6-well plate using 6 ml of DMEM solution and incubating at 37 °C and 5 % CO_2 for 72 h and 168 h under high humidity. The 6-well plates were agitated lightly for 5 s before and after the extract preparation process.

2.2.3. L929 cell culturing for biocompatibility profiling

L929 cells (Murine fibroblast) were used to study the biocompatibility profiles of the Ag/DLC coatings. Cell culture ingredients and reagents i.e., antibiotics, trypsin, FBS, and phosphate buffer saline were purchased from BioSera North America, Kansas City, MO, USA; Resazurin sodium salt was purchased from Fluorochem, UK; and plasticware including well plates and flasks were purchased from Corning, USA. The L929 cells were outsourced from Leibniz Institute DSMZ (Deutsche Sammlung von Mikroorganismen und Zellkulturen GmbH, Germany/German Collection of Microorganisms and Cell Cultures GmbH) and cultured in DMEM with addition of 10 % FBS, 100 μg/ml streptomycin, 100 U/ml penicillin, 2 mM L-glutamine, and high glucose. The cells were grown as a monolayer culture in a humidified incubator at 37 °C with 5 % CO_2. The cells were sub-cultured into a maximum of 15–20 passages until their confluency reached between 80 and 90 %.

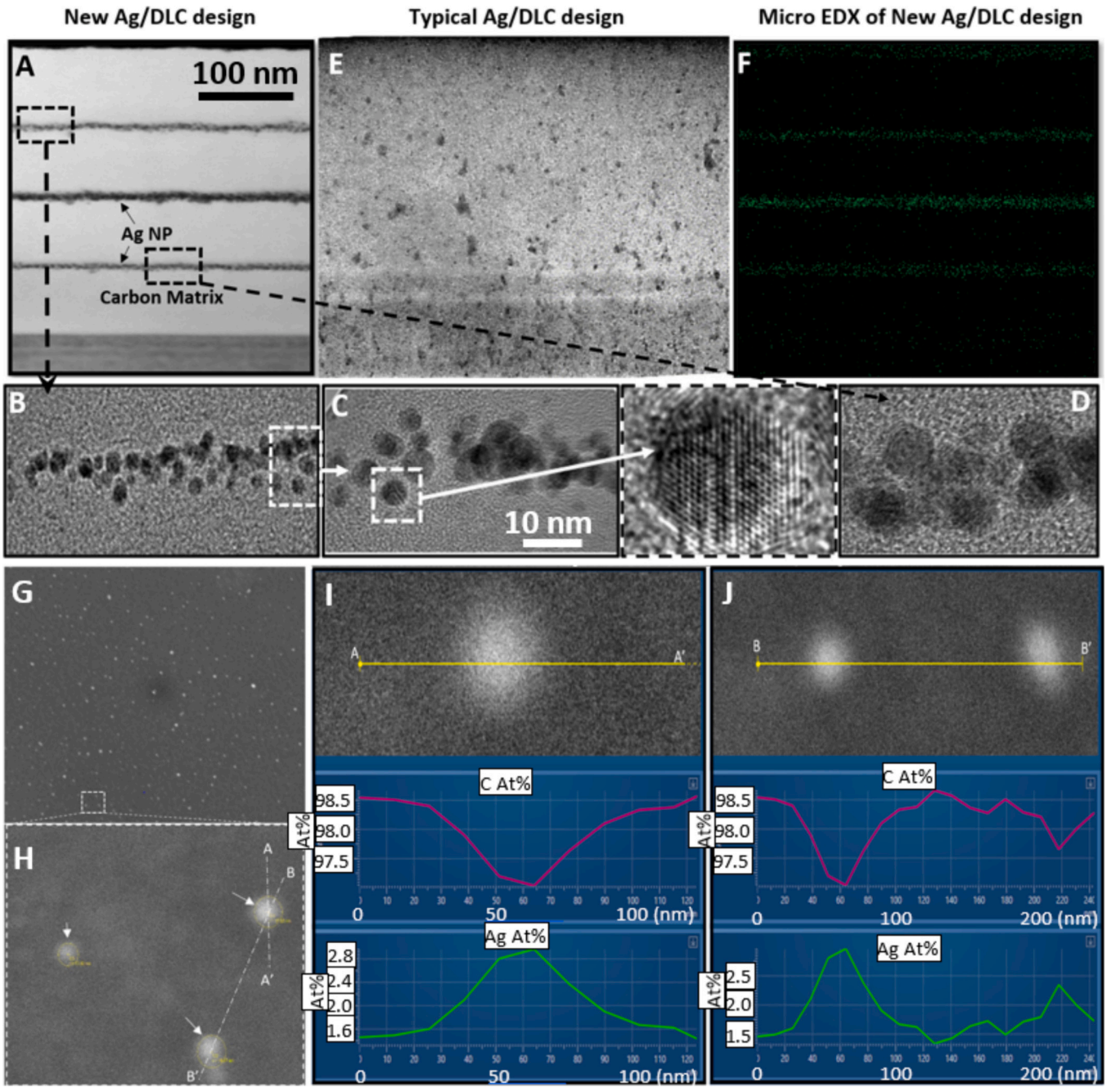

Fig. 2. TEM micrographs (A) Ag nanoparticles embedded in the DLC matrix at defined depths. (B–D) high-resolution images, including a single Ag nanoparticle, from the locations marked in (A). (E) A typical Ag/DLC, (F) corresponds to a chemical mapping of New Ag/DLC coating, where green lines depict the existence of Ag nanoparticles in the black DLC matrix. FESEM (G) low resolution and (H) high-resolution plane view micrographs of new Ag/DLC coatings and corresponding EDX line spectra of (I) single and (J) dual Ag nanoparticles as marked in (H).

2.3. Characterization of DLC and Ag/DLC coatings

2.3.1. Structural studies of DLC and Ag/DLC coatings

Structural studies of pure DLC, typical Ag/DLC, and new Ag/DLC coatings included coating thickness measurement, surface morphology, elemental compositions and mapping, and atomic structure studies. A Kapton tape was used to mask substrate for post-deposition thickness measurement studies. The coating thickness was measured at three different points for each sample using a Dektak XT contact surface profiler (Bruker Ltd.) with a 6 μm radius tip. The existence of embedded Ag nanoparticles at precise depths in the new Ag/DLC design was observed with focused ion beam (FIB) and transmission electron microscope (TEM) studies. The coating cross-section was prepared with a FIB (FEI Helios NanoLab 600 Dual Beam system) which uses a 30 keV Ga liquid metal ion source. The observations were made with a TEM (JEOL 2100F) at 200 keV and corresponding nanoscale elemental mapping was made with an integrated Oxford Instruments micros-analysis system at 200 keV and 0.7 nA. The surface morphology was observed with a field emission scanning electron microscope (FESEM, MIRA3, TESCAN) and the corresponding elemental compositions (large area to single Ag nanoparticle specific) were measured using electron dispersive X-ray spectroscopy (Oxford Instruments PLC, United Kingdom) coupled with the FESEM. The atomic structure was studied with Raman spectroscopy (Horiba LabRAM HR) performed in the range

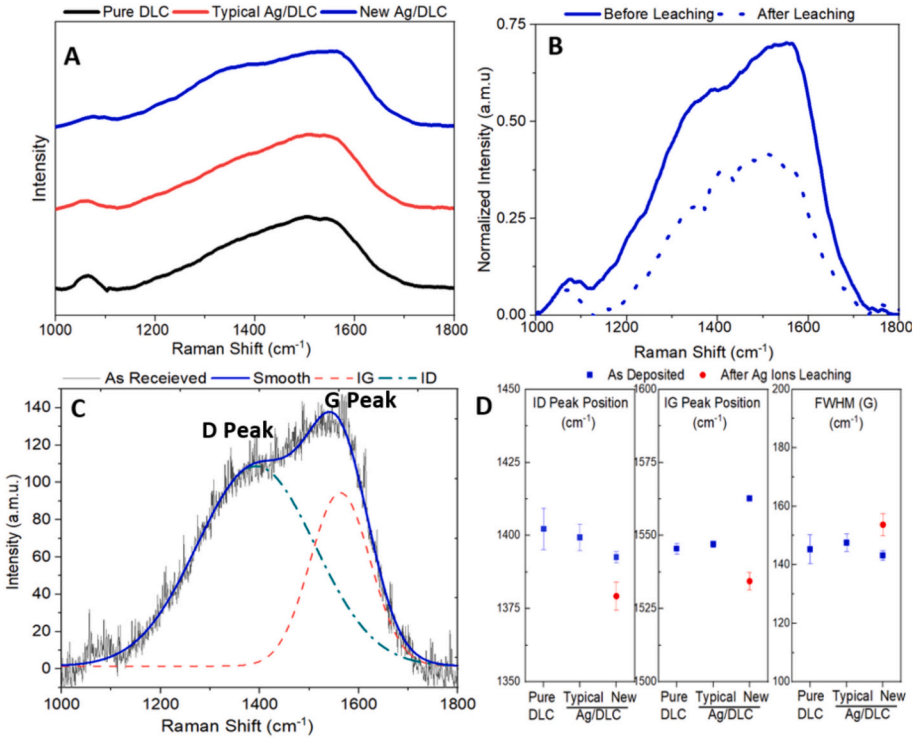

Fig. 3. (A) Raman spectra of as received pure DLC, typical Ag/DLC and new Ag/DLC coatings. (B) presents the change in atomic structure after ion leaching, (C) a representative example of deconvolution of Raman spectra and (D) corresponding values of ID, IG peak positions and FWHM (G) of pure DLC, typical Ag/DLC and new Ag/DLC coatings.

of 1150 to 1800 cm^{-1} using a 632.8 nm HeNe laser and 5 executions for each sample. The deconvolution analysis of Raman spectra was performed with OriginLab software to estimate ID, IG peak positions and Full Width of Half Maximum (FWHM) values.

2.3.2. Biocompatibility profiles of DLC and Ag/DLC coatings against L929 cells

Cu, Ti, and Ag ion concentrations were measured using leached extract of Cu and Ti controlled materials and typical and new Ag/DLC specimens after 72 h and 168 h in DMEM using inductively coupled plasma atomic emission spectroscopy (ICP-OES) using a Perkin Optima™ 8000 (Perkin Elmer, Inc.) ICP-OES Analyzer. The instrument was calibrated with 0.625, 2.5, 5.0 and 10.0 ppm known Ag, Ti, Cu concentrations that have demonstrated a correlation factor of 0.99. The spectroscopic analysis was performed at 327.393, 328.068 and 334.940 nm wavelengths for Cu, Ag and Ti.

The biocompatibility profiles of Cu, Ti, pure DLC, typical Ag/DLC, and new Ag/DLC coatings were investigated in compliance with ISO 10993 [21] using the Alamar Blue assay [22]. Cu is used as a positive control, Ti is used as a negative control, and pure DLC, typical Ag/DLC, and new Ag/DLC coatings were the points of interest. A 96-well culture plate was used, where 100 µL DMEM was poured into each well along with a cell density of 2000 per well. The cell culture plate was incubated overnight to promote cells adherence, and the next day, DMEM solution was replaced with leached extracts containing ions released from the materials under investigation. The biocompatibility profiles were measured at four (2^{*2}) experimental conditions i.e., (1) two leaching times of 72 h and 168 h and (2) two DMEM concentrations of for each leaching time i.e., undiluted DMEM solution and leached extracts 50 % diluted with blank DMEM. L929 cells were exposed to all four types of extracts for 72 h and then 10 µL of Resazurin (having a concentration of 1 mg/ml) was added to each well and further incubated for 4 h in dark conditions at 37 °C. The absorbance of treated extracts was measured at 570 and 600 nm wavelengths using a plate reader (Labtech LT5400, UK), while the cell viability was calculated [23] and expressed as a percentage of untreated (BLANK) cells. Further, the morphology of L929 cells that had been exposed to 168 h leached extracts for 72 h was observed with a Kern inverted microscope with a 10× lens and optically zoomed to 400×.

2.3.3. Mechanical properties of DLC and Ag/DLC coatings

The mechanical properties of pure DLC, typical Ag/DLC and new Ag/DLC coatings were studied using a nanoindenter (Hysitron TI900, Brukers Ltd.) with a Berkovich tip in compliance with ASTM C 1327–15 standard. 27 indentations were performed for each sample on the same parameters i.e., load-control indentation at 0.5 mN. The data was processed in MS Excel to find average values and standard deviations.

3. Results and discussion

3.1. Structural studies of DLC and Ag/DLC coatings

3.1.1. Coating morphology, and elemental composition

Fig. 2 presents the FESEM and TEM studies mainly for the new Ag/DLC to understand the difference in their microstructures with typical Ag/DLC. The depth-controlled doping of isolated Ag nanoparticles, the novelty of this study as illustrated in Fig. 1 can be visualized in Fig. 2A. Fig. 2B to D presents high-resolution micrographs of zones referred to Ag nanoparticle layers in Fig. 2A. The inset image in Fig. 2C presents a single Ag nanoparticle. It can be inferred that Ag nanoparticles are grown spherically. This design makes it different from typical co-sputtering where Ag is thoroughly doped in the carbon matrix from the substrate to the top of the matrix as shown in Fig. 2E. Fig. 2F presents a micro-elemental mapping of the same coating, where green bands present the existence of silver nanoparticles embedded at controlled depths in the black DLC coating matrix. The cross-section imaging depicts a layer of Ag nanoparticles due to particles detection from the rear, laying in the same horizontal plane. Therefore, their isolation could be

observed in high resolution images such as Fig. 2C for through plane views. Fig. 2G and H presents low-resolution and high-resolution plane view FESEM micrographs of the new Ag/DLC coatings, clearly showing that the isolated Ag nanoparticles are uniformly distributed across the surface. The typical Ag/DLC coatings have 83 at.% C and 17 at.% Ag (n = 3, SD ± 1), while the new Ag/DLC coatings have 98 at.% C and 2 at.% Ag (n = 3, SD ± 0.3), after removing contaminations originating from the glass substrate. Fig. 2I and J present the carbon and Ag atomic percentage of single and dual Ag nanoparticles along lines AA′ and BB′ as marked in Fig. 2H. The change in elemental composition of these Ag nanoparticles can be observed in the corresponding elemental line spectra. A large proportion of carbon is mainly detected from the background due to the difference in diameters of the electron beam (110 nm) and the small Ag nanoparticles.

3.1.2. Atomic structural studies

Fig. 3 presents the atomic structural studies of pure DLC, typical Ag/DLC, and new Ag/DLC coatings performed with Raman spectroscopy. Fig. 3A presents smoothened as-received Raman spectra of pure DLC and Ag/DLC coatings. The Raman spectra reflect bond disorders among carbon atoms, clustering of carbon sp^2 atoms, qualitative estimation of sp^2 rings and chains, and sp^2 and sp^3 proportions [24]. It can be observed that the Raman spectra of pure DLC and typical Ag/DLC coatings present a broad single G peak, depicting the amorphous structure of carbon films [25]. Whereas a shoulder peak (D peak) appeared in addition to a broad peak (G peak) in the new Ag/DLC coating, which suggests an increase in graphitic proportion [26,27]. The emergence of the ID shoulder peak with the addition of Ag nanoparticles is consistent with the literature [28,29]. Hence, a typical co-sputtering of Ag/DLC was conceived for making an amorphous structure while adding Ag in the form of isolated nanoparticles increases graphitic clustering and crystallinity in the new Ag/DLC coatings [25,30]. A small broad peak around 1100 cm^{-1} emerges from the glass substrate [31].

Fig. 3B presents the Raman spectra of new Ag/DLC coatings before and after preparing leached extracts, measured under the same testing conditions. It can be observed that the peak intensities are reduced after materials leaching. Generally, a decrease in peak intensities with material removal and an increase in peak intensities with material addition [32] are well documented in the literature. It is conceived that the structural porosity that emerged due to material removal during the leaching process has played a vital role in atomic excitations of carbon atoms. The porosity in carbon-based films have shown significant changes in Raman intensities when prepared for energy materials [33]. Specifically for in vivo applications of DLC and Ag/DLC coatings, the peak intensities are reported to increase due to the osteogenesis process which adds bone materials to DLC and Ag/DLC coatings [34]. Further, pure DLC and typical Ag/DLC coatings were completely dissolved in the extracts. Whereas the remnants of the new Ag/DLC reflect that the addition of Ag nanoparticles into the DLC matrix may have improved structural stability and adhesion of the coatings.

Fig. 3C presents a representative example of Gaussian multipeak deconvolution analysis performed in OriginLab software for pure DLC, typical Ag/DLC, and new Ag/DLC coatings. The peak positions and FWHM (G) values as mapped in Fig. 3D. The D peak position suggests breathing modes of sp^2 carbon atoms in rings while the G peak position suggests the relative motion of carbon sp^2 atoms [24,34] which are attributed to the disorder among carbon atoms. It can be seen that the pure DLC coating has the highest carbon atomic disorder which reduces for typical Ag/DLC and is further reduced for the new Ag/DLC coating. The D peak positions are in good agreement with Raman spectra as adding a higher amount of Ag has been shown to increase disorder in the carbon matrix [35].

The G peak positions and corresponding FWHM are used to estimate the degree of amorphous or graphitic structure and also to estimate DLC hardness [36]. A three-stage model [24,37] classifying carbon structures suggests G peak position of 1520 cm^{-1} corresponds to sp^2 a-C (ring structure) with a transition to ta-C (chain structure) until 1575 cm^{-1}. G peak positions of 1540 cm^{-1} suggest that the pure DLC and typical Ag/DLC coatings have a similar amorphous structure and are more inclined towards a ring structure. However, the addition of Ag nanoparticles to the DLC matrix has increased the carbon chain structures as the G peak shifts to ~1565 cm^{-1}. This increase in G peak position with the addition of Ag into DLC is also reported in the literature [38]. Similarly, the FHWM (G) corresponds to the crystallinity in the coatings. The amorphous carbon materials like DLC present broad peaks [39]. The degree of crystallinity increases with the reducing FWHM values [40], thus, crystalline carbon materials like diamond and graphene present narrow peaks [41]. The corresponding FWHM (G) results suggest that overall crystallinity in the coatings has increased after adding Ag nanoparticles to the DLC matrix. The increase in crystallinity is also validated with increased graphitic clustering in the coatings as presented by a shoulder peak in Fig. 3A. The literature also reflects a decrease in FWHM(G) with an increase in Ag concentration in the DLC matrix [42].

Referring to the behaviour of the new Ag/DLC coating after leaching, the D and G peak positions reduced and the FWHM (G) increased when compared to before leaching. The results suggest a relative increase in amorphization and aromatic rings in the coatings.

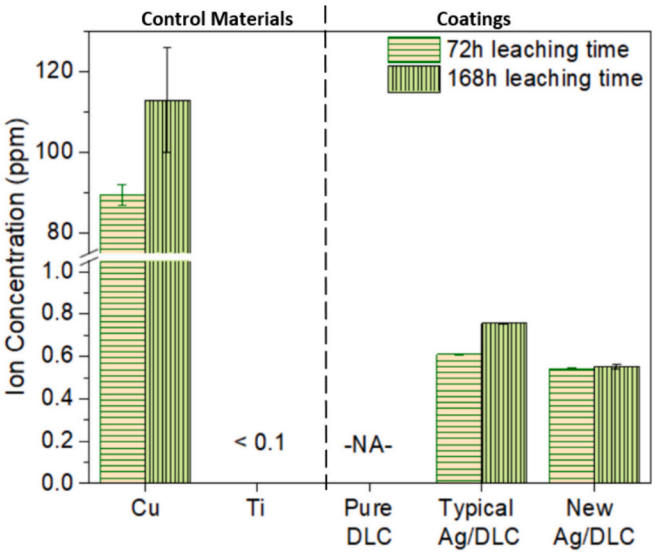

Fig. 4. Ion concentrations released from control materials and coatings during 72 h and 168 h leaching periods, measured with inductively coupled plasma-optical emission spectrometry (ICP-OES). New Ag/DLC coating with only 2 at.% Ag gives similar Ag ion release rate to typical Ag/DLC coating with 17 at.% Ag after 72 h of leaching.

3.2. Concentration of leached ions from control materials and coatings

Fig. 4 presents the concentration of Cu, Ti, and Ag ions leached from the control materials and coatings during 72 h and 168 h immersion times. It can be observed that Cu ion release rates were significantly higher than Ti and Ag from the Ag/DLC coatings. The Cu ion concentration was about 90 ppm and 112 ppm for 72 h and 168 h leaching times, respectively. The concentration of Ti ions released from the Ti substrate remained less than 0.1 ppm irrespective of leaching time. It was observed that the New Ag/DLC coating doped with only 2 at.% Ag gives a similar Ag ion release rate to Typical Ag/DLC coating with 17 at.% Ag of around 0.6 ppm after 72 h of leaching. A systematic study was previously performed [6] on the typical Ag/DLC design by varying Ag contents in the DLC matrix and mapping corresponding Ag ion leaching rates. Therefore, the value of 17 at.% Ag was selected in this study to develop a comparison between typical and new designs as it has shown similar ion release rates to 2 at.% Ag doped in the new Ag/DLC design.

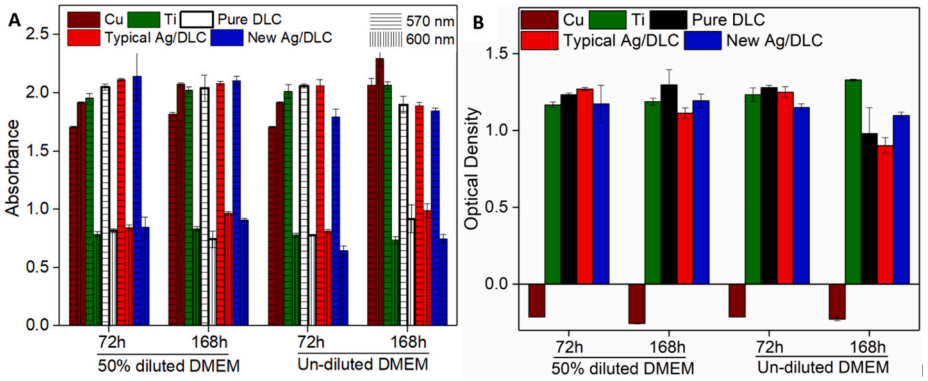

Fig. 5. (A) Absorbance and corresponding (B) optical densities of pure DLC, typical Ag/DLC and new Ag/DLC coatings. Where Cu and Ti are used as positive and negative controls, respectively.

Referring to the Ag ion concentration leached in 168 h, it can be observed that the typical Ag/DLC coating continued to release Ag ions, however, no further Ag ions were detected for the new Ag/DLC coating design. These patterns of Ag ion release are consistent with the Ag/DLC coating architectures based upon the amount of Ag doped into DLC matrix. The Ag ions continue to leach from the typical 17 at.% Ag/DLC coating as the Ag was doped throughout the DLC matrix. Whereas for the new 2 at.% Ag/DLC coating, all of the Ag was released in the early 72 h leaching period and nothing was measured for the next 96 h i.e. for the 168 h test. The literature [20] suggests that the Ag ion release rate from amorphous pure Ag coatings is lower than from Ag-doped carbon coatings and the difference reached to 100 % after 12 h. The Ag ions have only the opportunity to be released from the exterior/exposed surfaces of bulk materials, amorphous coatings, or clusters which is contrary to nanoparticles. The TEM micrographs present that the Ag exists with uncontrolled morphologies such as mixtures of particles, clusters, and agglomerations in the typical 17 at.% Ag/DLC coating, and therefore releases lower levels of Ag ions. In contrast, the isolated Ag nanoparticles in the new 2 at.% Ag/DLC coating exhibit larger surface area per unit volume, and therefore release higher levels of Ag ions. The rapid release of Ag ions is desirous in early post-surgery hours to perform swift antimicrobial actions. Ag ions are likely to release rapidly when silver nanoparticles are deposited on the surface or embedded close to the subsurface attributing to Ag ions mobility. The rapid release of Ag ions in the early hours of immersion rather than following hours is also well documented in literature [5,43]. In addition, a small concentration of Ag nanoparticles (less than 2.37 at.%) doped with a cluster beam technique have shown similar or higher Ag ion release rates when compared to co-sputtered Ag and carbon coatings having Ag concentration between 6.9 and 15.7 at.% [16].

3.3. Biocompatibility profiles of control materials and coatings

Biocompatibility studies of doped DLC coatings with L929 Cells (Murine fibroblast) are well adapted to investigate the biocompatibility of Ag/DLC [44], biological acceptance of CaO/DLC [45], cell viability of TiO_2/DLC [46] and Si/DLC [47], antimicrobial efficacy of ZnO/DLC [48], and cytotoxicity evaluation of dental endodontic pins [49]. Our study investigates the cell viability responses of pure DLC, typical and new Ag/DLC coatings against L929 cells.

3.3.1. Optical density measurements

Fig. 5A presents the absorbance and Fig. 5B presents the corresponding optical densities of 72 h and 168 h leached extracts treated with L929 cells for 72 h. The measurements performed at 570 nm wavelength present the absorbance at the start of treatment, while the measurements performed at 600 nm wavelength presents the absorbance at end of treatment. It can be observed that the absorbance

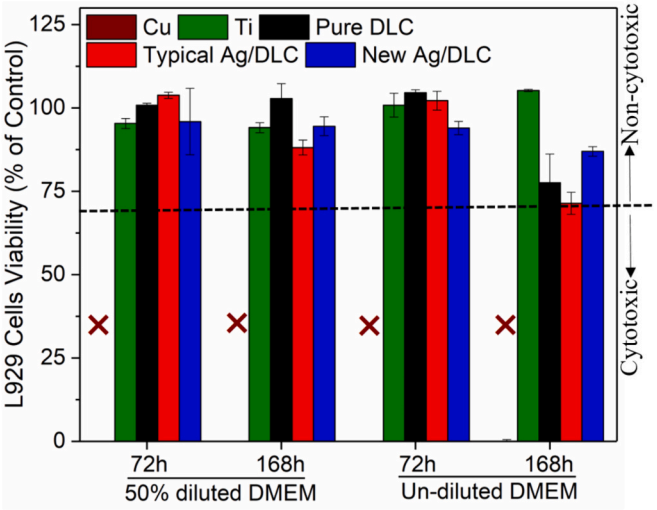

Fig. 6. Cell viability of typical Ag/DLC and new Ag/DLC coatings against L929 cell, treated for 72 h with 72 h and 168 h leached extracts. Whereas Cu and Ti are used as positive and negative controls, respectively.

reduced after the treatments except for the Cu positive control, which has shown a reverse trend when compared with all other materials under investigation. The increase in absorbance of positive controls and decrease in absorbance of negative controls has also been observed in the literature [50]. The amount of living and dead cells quantified in terms of absorbance is further used to estimate optical densities to be used as an indicator of biocompatibility, with increasing optical densities referring to higher cell adhesion [51]. It is well recognized that the living cells maintain good adhesion with coupons while the dead cells become nonadherent [52]. The optical density data suggests that the pure DLC and Ag/DLC coatings lose biocompatibility for undiluted 168 h leached extracts, when compared to all other conditions. Within the Ag/DLC coatings, the typical design has shown higher optical densities than the new Ag/DLC design for 72 h extractions. The possible higher cell decay is attributed to rapid Ag ion lease from the Ag nanoparticles exposed from the surface of the new Ag/DLC design, which is desirous in the early post-surgery period to respond against prospective infections. Further, the new Ag/DLC design has shown a safe and sustainable solution as the optical density of the new design has outperformed the typical Ag/DLC design for 168 h leached extracts, assuring better biocompatibility for long term potency of implants.

3.3.2. Cell viability profiles

The design criteria for biocompatibility of implantable devices

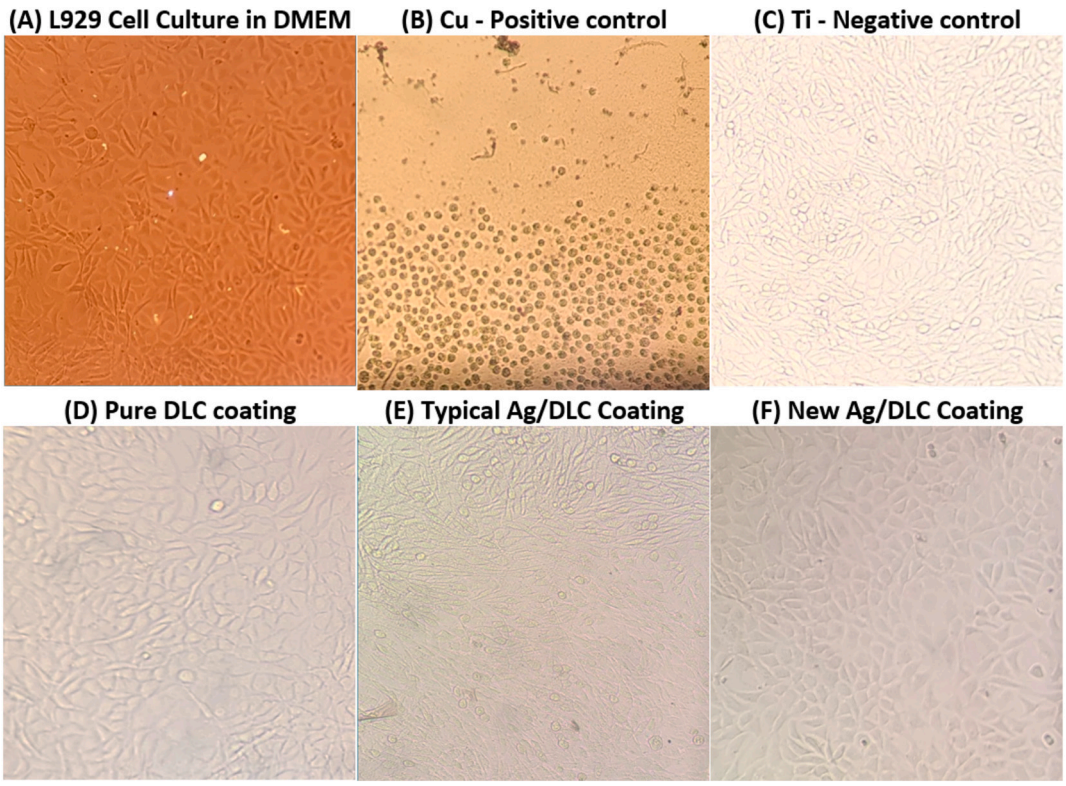

Fig. 7. L929 Cell morphologies after 72 h exposure to materials extracts prepared with 168 h leaching time. The living and dead cells have linear and circular morphologies, respectively. The new Ag/DLC coating design presents fewer dead cells and more living cells when compared to the typical Ag/DLC coating. All images are captured with a 10× lens and digitally enhanced to 400×.

suggests that they should be supporting the integration of host tissues rather than bacterial attachment and growth of biofilms; and also any antibacterial agents like Ag should not be exceeding systemic toxicity levels [53]. Therefore, the coatings should be toxic to unwanted microbes but should not be toxic to human cells. Hence, cell viability of 70 % of control draws a line between noncytotoxic and cytotoxic regimes, where a value above 70 % is considered non-cytotoxic (biocompatible) while a value lower than 70 % reflects that the biomaterial becomes cytotoxic [49,54]. The addition of Ag into DLC has shown a 99 % improvement in antibacterial effects in previous studies [55]. Further, Ag is also reported as a virucidal when tested against bovine rotavirus, adenovirus, herpes, and vaccinia viruses [56]. Therefore, Ag is a well-adopted antimicrobial agent for biomedical implants.

Fig. 6 presents L929 cell viability of the materials under investigation when 72 h and 168 h leached extracts were treated for 72 h. The Cu positive control has shown zero cell viability whereas the L929 cell viability of the Ti negative control remained close to 100 % irrespective of leaching time and DMDEM dilution. Referring to the pure DLC, typical Ag/DLC and new Ag/DLC coating profiles, it was observed that the cell viability was similar to the Ti negative control for 72 h leached extracts (irrespective of DMEM dilution) and for 168 h extracts diluted with 50 % DMEM. Whereas, the cell viability was reduced for all three coatings, pure DLC, typical Ag/DLC and new Ag/DLC for prolong 168 h leached with undiluted DMEM. It is conceived that more Ag ions are leached during the 168 h extraction in undiluted DMEM which is likely to reduce cell viability in comparison to 50 % diluted DMEM, where Ag ion concentrations per l were relatively reduced. Comparing typical and new Ag/DLC coatings, it was observed that the typical Ag/DLC coatings have more cell viability for 72 h leached extracts while the trend was revered for 168 h leached extracts. The cell viability response of Ag/DLC is attributed to the typical and new designs. The new Ag/DLC design exhibits a layer of isolated Ag particles on top of the DLC surface (as shown in Fig. 2F and G) which is likely to give robust Ag ion leaching when compared to the typical Ag/DLC design where Ag is embedded in DLC matrix. Hence, the cell viability was lower for the new Ag/DLC coating after 72 h leaching when compared to the typical Ag/DLC. Referring to the results for 168 h extracts, the Ag ions are continuously leached from the matrix as Ag was thoroughly doped into DLC in the typical Ag/DLC design, which is contrary to new Ag/DLC design, where only a small amount of Ag was doped in form of nanoparticles at precise locations. Hence, the continuous Ag ion release from the typical Ag/DLC design makes them borderline cytotoxic with only 71.36 ± 3.31 % cell viability, whereas the new Ag/DLC design remained biocompatible under the same conditions with a cell viability of 86.94 ± 1.44 %. The cell viability results suggest that adding Ag on top of the surface or near-surface in the form of nanoparticles can perform robust antimicrobial action which is desired for the early post-surgery period [57]. The C-reactive proteins which are considered inflammatory markers reach their highest value on the first day after surgery [58]. Hence, a short-term high dose of antimicrobial release was found desirous in the literature [57]. The literature also suggests that a sub-ppm Ag release is sufficient to induce antibacterial effects after a few hours when compared to larger values [53,59]. Similarly, the addition of Ag in carbon coatings in small concentrations like 1.1 at.% has shown to reduce human osteosarcoma (HOS) cell proliferation from 87 % to lower than 45 % (when compared with 100 % of control) [60]. The Ag potential for inactivating bacteria through surface contact even without releasing Ag ions has also been demonstrated in rare findings [61]. Therefore, it is anticipated that the new Ag/DLC design will not only provide adequate antimicrobial action in the early post-surgery hours but also give sufficient protection for up to three days (72 h) when host integration has already started. In contrast, the typical Ag/DLC design may develop a cytotoxic profile after three days due to the continuous release of Ag ions.

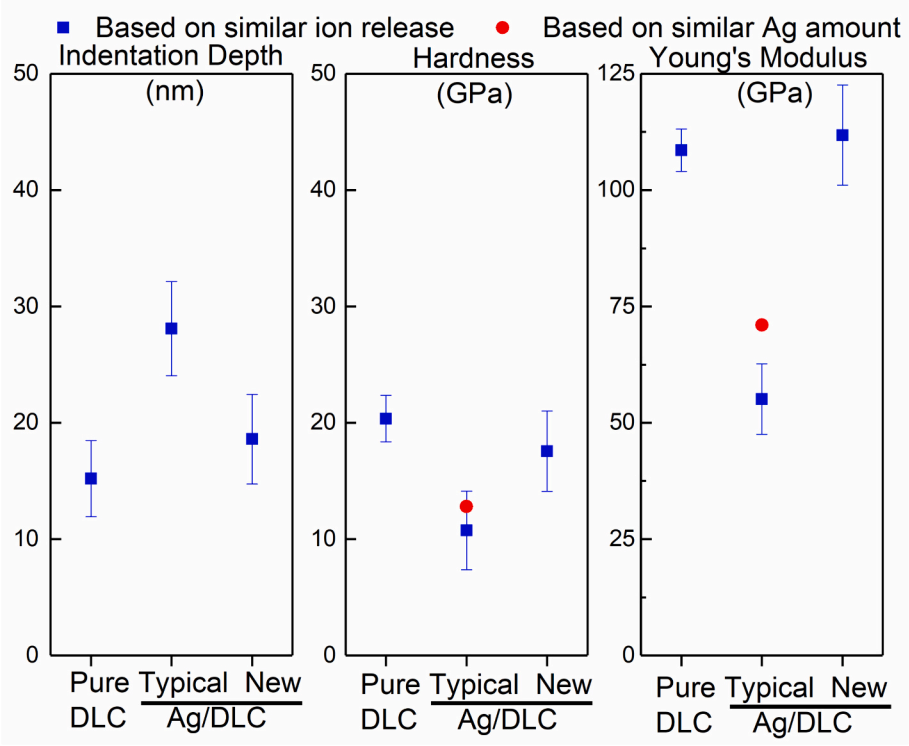

Fig. 8. Mechanical performance of typical and new Ag/DLC coatings compared on the bases of similar ion release rates (■ blue squares) and a similar amount of Ag doped into the DLC matrix (● red circles).

3.3.3. *Morphology of L929 cells before and after treatment*

Fig. 7 presents the morphologies of untreated L929 cells and those treated with 168 h leached extracts of Cu, Ti, pure DLC, typical Ag/DLC and new DLC coatings. It is well recognized that the linear morphology presents living cells while the dead cells become round [52]. All the L929 cells cultured in DMEM present linear morphologies as shown in Fig. 7A, with exception of one or two round spots which could be either dead cells, substrate features, or contamination. As expected, the Cu positive control has killed most of the cells as shown in Fig. 7B. Similarly, Fig. 7C presents the morphology of L929 cells against medical grade Ti, a negative control. It can be seen that most of the cells remained alive but several dead cells were also visible. Referring to the response of pure DLC against L929 cells in Fig. 7D, the cell viability was found to be similar to fresh DMEM cultured cells as DLC is well recognized for its biocompatibility. More living cells were observed per unit area at the surface of new Ag/DLC coating (Fig. 7F) when compared with typical Ag/DLC coatings (Fig. 7E). The qualitative comparison suggests a cell viability order from highest to lowest as: DMEM cultured cells, pure DLC, New Ag/DLC, Ti, Typical Ag/DLC, and Cu, respectively.

3.4. *Mechanical properties of pure DLC and Ag/DLC coatings*

Fig. 8 presents the mechanical properties i.e., indentation contact depth, hardness, and Young's modulus of typical and new Ag/DLC coatings compared on the bases of similar ion release rates and their performance against pure DLC coatings. Generally, the mechanical properties decline with the addition of Ag into the DLC matrix. Whereas, the typical Ag/DLC coating has presented more decline in hardness and Young's modulus when compared to new Ag/DLC model. The average contact depth for the pure DLC coating was 15 nm which increased to 28 nm for typical Ag/DLC and 18 nm for new Ag/DLC coatings. Correspondingly, the average hardness of the pure DLC coating was 20.3 GPa which reduced to 10.7 GPa (47 % decline) for typical Ag/DLC and 17.5 GPa (14 % decline) for new Ag/DLC coatings. Similarly, the pure DLC coating has an average Young's modulus of 109 GPa which reduced to 55 GPa (49 % decline) for typical Ag/DLC and slightly increased to 111 GPa (2 % increase) for new Ag/DLC coatings. The mechanical properties are attributed to the amount and morphology of Ag doped in the DLC coatings. The doping of small Ag crystallites in DLC have shown less decline in coating hardness when compared with large size Ag crystallites [62]. Similarly, a decrease in mechanical properties with increasing Ag amount in a DLC matrix is well reported in the literature. For example, the addition of 13 at.% Ag in DLC has shown a 28 % decline in hardness from 13 GPa to 9.3 GPa [38]. Similarly, another study has shown a 47 % decline in hardness from 9.5 GPa to 5 GPa with the addition of 12 at.% Ag in a DLC matrix [63]. Correspondingly, smaller Ag amounts doped in a DLC matrix have less impact on the overall mechanical properties of coatings. The Ag doping of 2.1 at.% in DLC has shown a reduction of only 6 % hardness i.e., 13.3 GPa to 12.4 GPa [4]. In a rare case, when Ag was doped in a DLC matrix using a mosaic target up to 2.99 at.% the DLC hardness increased by up to 40 % [64]. Similarly, smaller Ag amounts not only reduce the compromise on mechanical properties but also enhance coating life. Ag/DLC coatings with a lower Ag concentration like 3.24 at.% is recommended to give a lower friction coefficient when compared to a 10 at.% Ag/DLC coating [42]. The friction coefficient starts increasing [65], wear rate may double [5] and Ag/DLC coatings are likely to fail [38] against high contact stress when Ag is doped beyond 10 at.% in a DLC matrix. Hence, the mechanical properties of the typical and new Ag/DLC coatings are in good agreement with previous studies. The typical (17 at.%) and new (2 at.%) Ag/DLC coatings have similar ion release rates of ~0.6 ppm, but the new design has outperformed the typical Ag/DLC design with higher hardness and Young's modulus by 63 % and 100 %, respectively.

A comparison in the mechanical performance of typical and new Ag/DLC coatings was also attempted on the basis of similar Ag amount (2 at.%), instead of similar ion release rates (0.6 ppm). The deposition systems have limitations in depositing typical Ag/DLC coating with controlled doping of 2 at.% into the DLC matrix. Hence, the approximate hardness and Young's modulus of a typical Ag/DLC coating having 2 at.% Ag in the DLC matrix were deduced from curve fitting of Ag varied

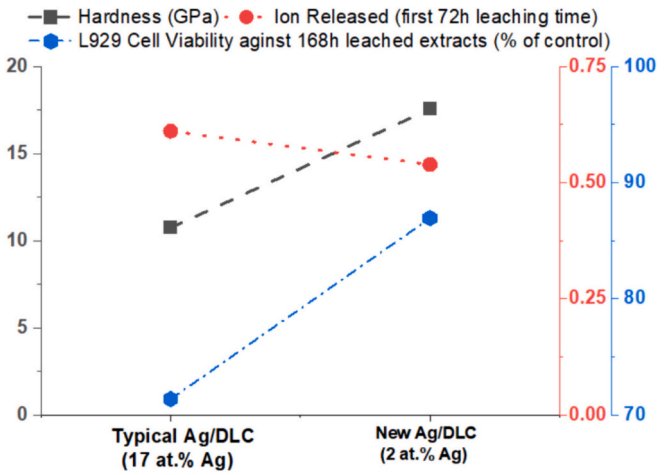

Fig. 9. Ag ion release levels and hardness of typical and new Ag/DLC coatings. The new Ag/DLC coating doped with only 2 at.% Ag releases similar Ag ion levels to the typical Ag/DLC coating doped with 17 at.% Ag. Correspondingly, the new Ag/DLC coating has 63 % higher hardness than the typical Ag/DLC coating.

Ag/DLC coatings fabricated as preliminary work. The linear curve fitting performed in OriginLab software calculates values of 12.8 GPa hardness and 71 GPa Young's modulus for a 2 at.% typical Ag/DLC coating (red circles in Fig. 8). The results suggest that when both coating designs are doped with the same amount of 2 at.% Ag, the typical Ag/DLC coating still lacks 27 % in hardness and 22 % in Young's modulus when compared with the new Ag/DLC design.

4. Overall performance of new Ag/DLC design

Fig. 9 and Table 1 present the overall performance of new Ag/DLC design. The outcomes suggest that depositing a small amount of Ag (i.e., 2 % in this study) in a DLC matrix in a new design (isolated Ag nanoparticles embedded at controlled depths) has shown improvements in mechanical properties, release similar concentrations of Ag ions and gives better biocompatibility profiles when compared to typical Ag/DLC doped with a higher amount of Ag i.e., 17 at.% in a DLC matrix. A 2 % s Ag when doped in a carbon matrix through a new design gives 63 % increase in hardness (10 to 17 GPa), 100 % higher Young's modulus (55 to 111 GPa), and 21 % higher biocompatibility (71 to 86 %) having a similar range of Ag ion release of 0.5 to 0.6 ppm as 17 at.% typical Ag/DLC. Table 1 reflects the biocompatibility of various Ag concentrations in DLC coatings investigated for their potential in anti-cancer, osteoblastic, and cardiovascular research using L929, EA.hy926, and SaOS-s cell lines. It can be observed that the higher amount of Ag makes Ag/DLC coating cytotoxic. A small amount of Ag ensures better biocompatibility irrespective of the cell line or deposition method and this study has further uplifted biocompatibility for the same amount of 2 at.% Ag, attributing to new coating design.

5. Conclusion

Silver doped diamond-like carbon coatings (Ag/DLC) coatings are typically made as a function of Ag contents doped throughout the DLC matrix. The excess of Ag not only reduces mechanical properties but may develop cytotoxicity profiles due to the continuous release of Ag ions. Whereas a sub-ppm Ag ion concentration has proven to provide adequate antimicrobial functioning in the literature. Hence, a new model of Ag/DLC coatings is proposed where the implicitly required amount of Ag is precisely doped in a DLC matrix in the form of nanoparticles with control over size, distribution and embedding depths. This work demonstrates that the New Ag/DLC coating doped with only 2 at.% Ag releases similar Ag ion levels to the Typical Ag/DLC coating doped with 17 at.% Ag. Ag nanoparticle specific EDX was performed to validate the presence of Ag nanoparticles in the new Ag/DLC coating, while Raman spectroscopy suggests that disorder in carbon atoms and graphitic clustering increases with the addition of Ag nanoparticles. It is observed that the Ag/DLC coating hardness and Young's modulus are less compromised contrary to typical Ag/DLC coatings, which is attributed to lower amounts of Ag doped in DLC matrix. However, the 2 at.% Ag doped with new design leaches similar Ag ion concentrations to the 17at% Ag doped in typical design. Biocompatibility profiles against L929 cells show that both the typical and new Ag/DLC coatings remained biocompatible when treated against undiluted 72 h leached extracts and 168 h leached extracts diluted with DMEM. The new Ag/DLC coatings have shown a robust antimicrobial potential during the first 72 h of cell exposure, which is desirous to fight potential inflammation in the early post-surgery period. At the extreme conditions of undiluted DMEM and 168 h leached extracts, the typical Ag/DLC coating becomes borderline cytotoxic with a cell viability of 71 % of control, while the new Ag/DLC coating remained biocompatible with a cell viability of 86 % of control. The new Ag/DLC design has shown outstanding potential to develop the next generation of high-performance Ag/DLC coatings for bio-mechanical applications, particularly for invasive load-carrying orthopaedic implants.

CRediT authorship contribution statement

Abdul Wasy Zia: Writing – review & editing, Writing – original draft, Investigation, Funding acquisition, Formal analysis, Data curation, Conceptualization. **Ioannis Anestopoulos:** Formal analysis, Data curation. **Leon Bowen:** Data curation. **Mihalis I. Panayiotidis:** Writing – review & editing, Supervision, Resources. **Martin Birkett:** Writing – review & editing, Supervision, Resources, Project administration, Funding acquisition.

Declaration of competing interest

The authors declare that they have no competing interests.

Table 1
Cell viability as a function of silver amount doped in carbon coating.

Serial	Ag/DLC deposition method	Cell viability (% of control)	Silver amount in carbon coating (%)	Exposure time (h)	Cell line	Potential application	Reference
1	Sputtering	0	65	168	L929	Anti-cancer research	[6]
2	Sputtering	25	40	168	L929		
3	Sputtering	71	17	168	L929		
4	Ion implantation + sputtering	50	9	48	EA. hy926	Cardiovascular research	[11]
5	Ion implantation + sputtering	70	5	48	EA. hy926		[11]
6	Filtered cathodic arc	82.5	2	24	SaOS-2	Osteoblastic research	[7]
7	Sputtering	86	2	168	L929	Anti-cancer research	This study

Data availability

The dataset generated during and/or analyzed during the current study is available in the Figshare repository, DOI: https://doi.org/10.25398/rd.northumbria.21388734.v1.

Acknowledgment

This project has received funding from the European Union's Horizon 2020 research and innovation programme under the Marie Sklodowska-Curie Grant Agreement No 885534. The work was carried during AWZ's MSCA-IF Fellowship at Northumbria University from 02/2021 to 02/2023.

References

[1] R.K. Roy, K.-R. Lee, Biomedical applications of diamond-like carbon coatings: a review, Journal of Biomedical Materials Research Part B: Applied, Biomaterials 83B (1) (2007) 72–84.
[2] S.P. Deshmukh, S.M. Patil, S.B. Mullani, S.D. Delekar, Silver nanoparticles as an effective disinfectant: a review, Mater. Sci. Eng. C 97 (2019) 954–965.
[3] X. Yu, Y. Qin, C. Wang, Y. Yang, X. Ma, Effects of nanocrystalline silver incorporation on sliding tribological properties of Ag-containing diamond-like carbon films in multi-ion beam assisted deposition, Vacuum 89 (2013) 82–85.
[4] L.J. Wang, F. Zhang, A. Fong, K.M. Lai, P.W. Shum, Z.F. Zhou, Z.F. Gao, T. Fu, Effects of silver segregation on sputter deposited antibacterial silver-containing diamond-like carbon films, Thin Solid Films 650 (2018) 58–64.
[5] S. Domínguez-Meister, T.C. Rojas, J.E. Frías, J.C. Sánchez-López, Silver effect on the tribological and antibacterial properties of a-C:Ag coatings, Tribol. Int. 140 (2019) 105837.
[6] A.W. Zia, I. Anestopoulos, M.I. Panayiotidis, L. Bowen, M. Birkett, Biomechanical characteristics of silver enriched diamond-like carbon coatings for medical applications, J. Alloys Compd. 958 (2023) 170473.
[7] J. Orrit-Prat, R. Bonet, E. Rupérez, M. Punset, M. Ortiz-Hernández, J. Guillem-Marti, A. Lousa, D. Cano, C. Díaz, G. García Fuentes, J. Caro, Bactericidal silver-doped DLC coatings obtained by pulsed filtered cathodic arc co-deposition, Surf. Coat. Technol. 411 (2021) 126977.
[8] C. Liao, Y. Li, S.C. Tjong, Bactericidal and cytotoxic properties of silver nanoparticles, Int. J. Mol. Sci. 20 (2) (2019) 449.
[9] L. Xu, Y.-Y. Wang, J. Huang, C.-Y. Chen, Z.-X. Wang, H. Xie, Silver nanoparticles: synthesis, medical applications and biosafety, Theranostics 10 (20) (2020) 8996–9031.
[10] M. Birkett, L. Dover, C. Cherian Lukose, A. Wasy Zia, M.M. Tambuwala, Á. Serrano-Aroca, Recent advances in metal-based antimicrobial coatings for high-touch surfaces, Int. J. Mol. Sci. 23 (3) (2022) 1162.
[11] D. Bociaga, P. Komorowski, D. Batory, W. Szymanski, A. Olejnik, K. Jastrzebski, W. Jakubowski, Silver-doped nanocomposite carbon coatings (Ag-DLC) for biomedical applications – physiochemical and biological evaluation, Appl. Surf. Sci. 355 (2015) 388–397.
[12] W. Zhang, Y. Yao, N. Sullivan, Y. Chen, Modeling the primary size effects of citrate-coated silver nanoparticles on their ion release kinetics, Environ. Sci. Technol. 45 (10) (2011) 4422–4428.
[13] M. Cloutier, S. Turgeon, Y. Busby, M. Tatoulian, J.J. Pireaux, D. Mantovani, Controlled distribution and clustering of silver in Ag-DLC nanocomposite coatings using a hybrid plasma approach, ACS Appl. Mater. Interfaces 8 (32) (2016) 21020–21027.
[14] S.A. Salehizadeh, R. Serra, I. Carvalho, A. Cavaleiro, S. Carvalho, Development of nanocomposite coating by hybrid gas condensation process and magnetron sputtering equipment: electrochemical characteristics and surface analysis, J. Mater. Eng. Perform. 30 (6) (2021) 4083–4093.
[15] I. Carvalho, M. Faraji, A. Ramalho, A.P. Carvalho, S. Carvalho, A. Cavaleiro, Ex-vivo studies on friction behaviour of ureteral stent coated with Ag clusters incorporated in a:C matrix, Diam. Relat. Mater. 86 (2018) 1–7.
[16] G. Sanzone, S. Field, D. Lee, J. Liu, P. Ju, M. Wang, P. Navabpour, H. Sun, J. Yin, P. Lievens, Antimicrobial and aging properties of Ag-, Ag/Cu-, and Ag cluster-doped amorphous carbon coatings produced by magnetron sputtering for space applications, ACS Appl. Mater. Interfaces 14 (8) (2022) 10154–10166.
[17] O.A. Streletskiy, I.A. Zavidovskiy, O.Y. Nischak, A.A. Haidarov, Size control of silver nanoclusters during ion-assisted pulse-plasma deposition of carbon-silver composite thin films, Vacuum 175 (2020) 109286.
[18] D. Merker, B. Popova, T. Bergfeldt, T. Weingärtner, G.H. Braus, J.P. Reithmaier, C. Popov, Antimicrobial propensity of ultrananocrystalline diamond films with embedded silver nanodroplets, Diam. Relat. Mater. 93 (2019) 168–178.
[19] A.W. Zia, I. Anestopoulos, M.I. Panayiotidis, M. Birkett, Soft diamond-like carbon coatings with superior biocompatibility for medical applications, Ceram. Int. 49 (11, Part A) (2023) 17203–17211.
[20] N.K. Manninen, S. Calderon, I. Carvalho, M. Henriques, A. Cavaleiro, S. Carvalho, Antibacterial Ag/a-C nanocomposite coatings: the influence of nano-galvanic a-C and Ag couples on Ag ionization rates, Appl. Surf. Sci. 377 (2016) 283–291.
[21] I. 10993-1, Biological Evaluation of Medical Devices—Part 1: Evaluation and Testing Within a Risk Management Process, International Organization for Standardization Geneva, Switzerland, 2018.
[22] C.C. Lukose, I. Anestopoulos, T. Mantso, L. Bowen, M.I. Panayiotidis, M. Birkett, Thermal activation of Ti(1-x)Au(x) thin films with enhanced hardness and biocompatibility, Bioactive Materials 15 (2022) 426–445.
[23] M. Singh, R.K. Singh, S.K. Singh, S.K. Mahto, N. Misra, In vitro biocompatibility analysis of functionalized poly(vinyl chloride)/layered double hydroxide nanocomposites, RSC Adv. 8 (71) (2018) 40611–40620.
[24] A.C. Ferrari, J. Robertson, Interpretation of Raman spectra of disordered and amorphous carbon, Phys. Rev. B 61 (20) (2000) 14095–14107.
[25] K. Baba, R. Hatada, S. Flege, W. Ensinger, Preparation and properties of Ag-containing diamond-like carbon films by magnetron plasma source ion implantation, Adv. Mater. Sci. Eng. 2012 (2012) 536853.
[26] S. Kurita, A. Yoshimura, H. Kawamoto, T. Uchida, K. Kojima, M. Tachibana, P. Molina-Morales, H. Nakai, Raman spectra of carbon nanowalls grown by plasma-enhanced chemical vapor deposition, J. Appl. Phys. 97 (10) (2005) 104320.
[27] M. Panda, G. Mangamma, R. Krishnan, K.K. Madapu, D.N.G. Krishna, S. Dash, A. K. Tyagi, Nano scale investigation of particulate contribution to diamond like carbon film by pulsed laser deposition, RSC Adv. 6 (8) (2016) 6016–6028.
[28] G. Zakarienė, A. Novoslavskij, Š. Meškinis, A. Vasiliauskas, A. Tamulevičienė, S. Tamulevičius, T. Alter, M. Malakauskas, Diamond like carbon Ag nanocomposites as a control measure against Campylobacter jejuni and Listeria monocytogenes on food preparation surfaces, Diam. Relat. Mater. 81 (2018) 118–126.
[29] H.W. Choi, J.-H. Choi, K.-R. Lee, J.-P. Ahn, K.H. Oh, Structure and mechanical properties of Ag-incorporated DLC films prepared by a hybrid ion beam deposition system, Thin Solid Films 516 (2) (2007) 248–251.
[30] F.R. Marciano, L.F. Bonetti, L.V. Santos, N.S. Da-Silva, E.J. Corat, V.J. Trava-Airoldi, Antibacterial activity of DLC and Ag–DLC films produced by PECVD technique, Diam. Relat. Mater. 18 (5) (2009) 1010–1014.
[31] D. Tuschel, Why are the Raman spectra of crystalline and amorphous solids different? Spectroscopy 32 (3) (2017) 26–33.
[32] N. Moolsradoo, S. Watanabe, Influence of elements on the corrosion resistance of DLC films, Adv. Mater. Sci. Eng. 2017 (2017) 3571454.
[33] J. Song, L. Wang, Z. Ma, Z. Du, G. Shao, L. Kong, W. Gao, Biotemplated fabrication of a novel hierarchical porous C/LiFePO4/C composite for Li-ion batteries, RSC Adv. 5 (3) (2015) 1983–1988.
[34] M.d.V.E.A. Ankha, A.d.M. Silva, R.F.d. Prado, M.P. Camalionte, L.M.R. d. Vasconcellos, P.A. Radi, A.S.d. Silva, L. Vieira, Y.R. Carvalho, Effect of DLC films with and without silver nanoparticles deposited on titanium alloy, Braz. Dent. J. 30 (2019) 607–616.
[35] L. Duta, C. Ristoscu, G.E. Stan, M.A. Husanu, C. Besleaga, M.C. Chifiriuc, V. Lazar, C. Bleotu, F. Miculescu, N. Mihailescu, E. Axente, M. Badiceanu, D. Bociaga, I. N. Mihailescu, New bio-active, antimicrobial and adherent coatings of nanostructured carbon double-reinforced with silver and silicon by Matrix-Assisted Pulsed Laser Evaporation for medical applications, Appl. Surf. Sci. 441 (2018) 871–883.
[36] N. Ohtake, M. Hiratsuka, K. Kanda, H. Akasaka, M. Tsujioka, K. Hirakuri, A. Hirata, T. Ohana, H. Inaba, M. Kano, H. Saitoh, Properties and classification of diamond-like carbon films, Materials 14 (2) (2021).
[37] A.C. Ferrari, S.E. Rodil, J. Robertson, Interpretation of infrared and Raman spectra of amorphous carbon nitrides, Phys. Rev. B 67 (15) (2003) 155306.
[38] N.K. Manninen, F. Ribeiro, A. Escudeiro, T. Polcar, S. Carvalho, A. Cavaleiro, Influence of Ag content on mechanical and tribological behavior of DLC coatings, Surf. Coat. Technol. 232 (2013) 440–446.
[39] C. Srisang, P. Asanithi, K. Siangchaew, S. Limsuwan, A. Pokaipisit, P. Limsuwan, Raman spectroscopy of DLC/a-Si bilayer film prepared by pulsed filtered cathodic arc, J. Nanomater. 2012 (2012) 745126.
[40] R. Zarei Moghadam, H. Rezagholipour Dizaji, M.H. Ehsani, Modification of optical and mechanical properties of nitrogen doped diamond-like carbon layers, J. Mater. Sci. Mater. Electron. 30 (22) (2019) 19770–19781.
[41] R. Kalish, A. Reznik, K.W. Nugent, S. Prawer, The nature of damage in ion-implanted and annealed diamond, Nucl. Instrum. Methods Phys. Res., Sect. B 148 (1) (1999) 626–633.
[42] P.P. Jing, D.L. Ma, Y.L. Gong, X.Y. Luo, Y. Zhang, Y.J. Weng, Y.X. Leng, Influence of Ag doping on the microstructure, mechanical properties, and adhesion stability of diamond-like carbon films, Surf. Coat. Technol. 405 (2021) 126542.
[43] C. Gorzelanny, R. Kmeth, A. Obermeier, A.T. Bauer, N. Halter, K. Kümpel, M. F. Schneider, A. Wixforth, H. Gollwitzer, R. Burgkart, B. Stritzker, S.W. Schneider, Silver nanoparticle-enriched diamond-like carbon implant modification as a mammalian cell compatible surface with antimicrobial properties, Sci. Rep. 6 (1) (2016) 22849.
[44] A.A. Vieira, T.B. Santos, M.G. Silva, L.A. Manfroi, N.S. Silva, P. Leite, L. Vieira, P.A. Radi, S.F. Santos, J.V.C.d. Souza, A comparison of biocompatibility and Osseointegration on ceramic with and without DLC-Ag films: an in vitro study, Proceedings of the 18. Brazil MRS Meeting 2019, 2019.
[45] A. Dorner-Reisel, C. Schürer, G. Irmer, F. Simon, C. Nischan, E. Müller, Diamond-like carbon coatings with Ca-O-incorporation for improved biological acceptance, Anal. Bioanal. Chem. 374 (4) (2002) 753–755.
[46] F.R. Marciano, C.C. Wachesk, A.O. Lobo, V.J. Trava-Airoldi, C. Pacheco-Soares, N. S. Da-Silva, Thermodynamic aspects of fibroblastic spreading on diamond-like carbon films containing titanium dioxide nanoparticles, Theor. Chem. Accounts 130 (4) (2011) 1085–1093.

[47] S. Movahed, A.K. Nguyen, P.L. Goering, S.A. Skoog, R.J. Narayan, Argon and oxygen plasma treatment increases hydrophilicity and reduces adhesion of silicon-incorporated diamond-like coatings, Biointerphases 15 (4) (2020) 041007.
[48] S. Buchegger, A. Kamenac, S. Fuchs, R. Herrmann, P. Houdek, C. Gorzelanny, A. Obermeier, S. Heller, R. Burgkart, B. Stritzker, A. Wixforth, C. Westerhausen, Smart antimicrobial efficacy employing pH-sensitive ZnO-doped diamond-like carbon coatings, Sci. Rep. 9 (1) (2019) 17246.
[49] V. Cannella, R. Altomare, G. Chiaramonte, S. Di Bella, F. Mira, L. Russotto, P. Pisano, A. Guercio, Cytotoxicity evaluation of endodontic pins on L929 cell line, Biomed. Res. Int. 2019 (2019) 3469525.
[50] C. da Silva, C. Soares, W. Joaquim, R. Menegon, Mitochondrial activity and cell damage after application of Acmella oleracea leaf extract, American, Journal of Plant Sciences 7 (2016) 2498–2504.
[51] F.-P. Lee, D.-J. Wang, L.-K. Chen, C.-M. Kung, Y.-C. Wu, K.-L. Ou, C.-H. Yu, Antibacterial nanostructured composite films for biomedical applications: microstructural characteristics, biocompatibility, and antibacterial mechanisms, Biofouling 29 (3) (2013) 295–305.
[52] A. Isakovic, Z. Markovic, B. Todorovic-Markovic, N. Nikolic, S. Vranjes-Djuric, M. Mirkovic, M. Dramicanin, L. Harhaji, N. Raicevic, Z. Nikolic, V. Trajkovic, Distinct cytotoxic mechanisms of pristine versus hydroxylated fullerene, Toxicol. Sci. 91 (1) (2006) 173–183.
[53] M. Cloutier, R. Tolouei, O. Lesage, L. Lévesque, S. Turgeon, M. Tatoulian, D. Mantovani, On the long term antibacterial features of silver-doped diamondlike carbon coatings deposited via a hybrid plasma process, Biointerphases 9 (2) (2014) 029013.
[54] G.K. Srivastava, M.L. Alonso-Alonso, I. Fernandez-Bueno, M.T. Garcia-Gutierrez, F. Rull, J. Medina, R.M. Coco, J.C. Pastor, Comparison between direct contact and extract exposure methods for PFO cytotoxicity evaluation, Sci. Rep. 8 (1) (2018) 1425.
[55] S.C.H. Kwok, W. Zhang, G.J. Wan, D.R. McKenzie, M.M.M. Bilek, P.K. Chu, Hemocompatibility and anti-bacterial properties of silver doped diamond-like carbon prepared by pulsed filtered cathodic vacuum arc deposition, Diam. Relat. Mater. 16 (4) (2007) 1353–1360.
[56] U. Klueh, V. Wagner, S. Kelly, A. Johnson, J.D. Bryers, Efficacy of silver-coated fabric to prevent bacterial colonization and subsequent device-based biofilm formation, J. Biomed. Mater. Res. 53 (6) (2000) 621–631.
[57] M. Cloutier, D. Mantovani, F. Rosei, Antibacterial coatings: challenges, perspectives, and opportunities, Trends Biotechnol. 33 (11) (2015) 637–652.
[58] Y. Abe, M. Chiba, S. Yaklai, R.S. Pechayco, H. Suzuki, T. Takahashi, Increase in bone metabolic markers and circulating osteoblast-lineage cells after orthognathic surgery, Sci. Rep. 9 (1) (2019) 20106.
[59] A. Mazare, A. Anghel, C. Surdu-Bob, G. Totea, I. Demetrescu, D. Ionita, Silver doped diamond-like carbon antibacterial and corrosion resistance coatings on titanium, Thin Solid Films 657 (2018) 16–23.
[60] W. Tillmann, N.F. Lopes Dias, C. Franke, D. Kokalj, D. Stangier, V. Filor, R. H. Mateus-Vargas, H. Oltmanns, M. Kietzmann, J. Meißner, M. Hein, S. Pramanik, K.-P. Hoyer, M. Schaper, A. Nienhaus, C.A. Thomann, J. Debus, Tribo-mechanical properties and biocompatibility of Ag-containing amorphous carbon films deposited onto Ti6Al4V, Surf. Coat. Technol. 421 (2021) 127384.
[61] S. Rtimi, S. Konstantinidis, N. Britun, V. Nadtochenko, I. Khmel, J. Kiwi, New evidence for Ag-sputtered materials inactivating bacteria by surface contact without the release of Ag ions: end of a long controversy? ACS Appl. Mater. Interfaces 12 (4) (2020) 4998–5007.
[62] W. Tillmann, N.F. Lopes Dias, D. Stangier, A. Nienhaus, C.A. Thomann, A. Wittrock, H. Moldenhauer, J. Debus, Effect of the bias voltage on the structural and tribo-mechanical properties of Ag-containing amorphous carbon films, Diam. Relat. Mater. 105 (2020) 107803.
[63] Y. Wu, J. Chen, H. Li, L. Ji, Y. Ye, H. Zhou, Preparation and properties of Ag/DLC nanocomposite films fabricated by unbalanced magnetron sputtering, Appl. Surf. Sci. 284 (2013) 165–170.
[64] P.P. Jing, Y.L. Gong, Q.Y. Deng, Y.Z. Zhang, N. Huang, Y.X. Leng, The formation of the "rod-like wear debris" and tribological properties of Ag-doped diamond-like carbon films fabricated by a high-power pulsed plasma vapor deposition technique, Vacuum 173 (2020) 109125.
[65] Z. Zhao, X. Yu, Z. Zhang, W. Shu, J. Li, Attempting AG-doped diamond-like carbon film to improve seal performance of hydraulic servo-actuator, Materials 13 (11) (2020).